IOP Conf. Series: Materials Science and Engineering **143** (2016) 012023 doi:10.1088/1757-899X/143/1/012023

Contactless inductive flow tomography: basic principles and first applications in the experimental modelling of continuous casting

F Stefani, S Eckert, M Ratajczak, K Timmel and T Wondrak
Helmholtz-Zentrum Dresden – Rossendorf, Bautzner Landstraße 400, 01328 Dresden, Germany

E-mail: F.Stefani@hzdr.de

Abstract. Contactless inductive flow tomography (CIFT) aims at reconstructing the flow structure of a liquid metal from the magnetic fields measured at various positions outside the fluid body which are induced by the flow under the influence of one or multiple applied magnetic fields. We recap the basic mathematical principles of CIFT and the results of an experiment in which the propeller-driven three-dimensional flow in a cylindrical had been reconstructed. We also summarize the recent activities to utilize CIFT in various problems connected with the experimental simulation of the continuous casting process. These include flow reconstructions in single-phase and two-phase flow problems in the Mini-LIMMCAST model of slab-casting, studies of the specific effects of an electromagnetic stirrer attached to the Submerged Entry Nozzle (SEN), as well as first successful applications of CIFT on the background of a strong electromagnetic brake field. We conclude by discussing some remaining obstacles for the deployment of CIFT in a real caster.

1. Introduction

In many metallurgical technologies it is desirable to monitor the velocity field of the liquid metal. Its opaqueness usually prevents the deployment of optical measurement techniques, such as laser Doppler anemometry (LDA) or particle image velocimetry (PIV). Non-optical flow measurement techniques, using ultrasonic beams or intrusive pressure or potential probes, face serious problems if the liquid metal is hot and/or chemically aggressive. Any sort of contactless flow measurement would be most helpful in these cases.

The contactless inductive flow tomography (CIFT) [1] is able to provide a rough picture of the flow by applying primary magnetic fields to the metallic melt and by measuring the flow induced (secondary) magnetic field perturbation outside the fluid volume. The primary magnetic field can be applied in various directions. This allows collecting more information about (basically) the same velocity field, as long as the typical time for velocity changes is larger than the switching times between different applied fields. The remaining non-uniqueness of the inverse problem can be overcome by using standard regularization methods, such as Tikhonov regularization and the L-curve technique [2].

We start by delineating the basic mathematics for the forward and the inverse problem as it had been developed in previous publications [3-5]. In Section 3, we recap the results of a first test experiment which had shown the applicability of CIFT for the reconstruction of three-dimensional

velocity fields [1]. With view on the application to the continuous casting of steel, we focus then on the reduction of CIFT to the (essentially) two-dimensional (2D) geometry of slab-casting for which some experimental results are illustrated. We also present some new results evidencing the feasibility of CIFT in the presence of a strong magnetic brake field. The paper concludes with an outlook on future methodological developments and possible industrial implementations of CIFT.

2. Basic mathematics

In this section we give a short outline of the basic mathematics underlying CIFT. We consider an electrically conductive fluid with a velocity field **u,** that is assumed to be steady or at least slowly varying on the magnetic diffusion time scale. Imagine this moving fluid to be exposed to a stationary magnetic field **B**. Then, according to Ohm's law in moving conductors, the current density

$$\mathbf{j} = \sigma(\mathbf{u}\times\mathbf{B} - \nabla\varphi) \tag{1}$$

is induced, where σ is the electrical conductivity of the fluid and φ denotes the electric scalar potential. According to Biot-Savart's law, this current density **j** induces now a secondary magnetic field **b** at a position **r**:

$$\mathbf{b}(\mathbf{r}) = \frac{\sigma\mu_0}{4\pi}\int_D \frac{\big(\mathbf{u}(\mathbf{r}')\times\mathbf{B}(\mathbf{r}')\big)\times(\mathbf{r}-\mathbf{r}')}{|\mathbf{r}-\mathbf{r}'|^3}\,dV' + \frac{\sigma\mu_0}{4\pi}\oiint_S \varphi(\mathbf{s}')\,\frac{\mathbf{r}-\mathbf{s}'}{|\mathbf{r}-\mathbf{s}|^3}\times\mathbf{n}(\mathbf{s}')dS' \tag{2}$$

In the volume integral, dV' denotes the volume element and $\mathbf{r}'$ the position vector in the volume. In the surface integral, dS' denotes a surface element and $\mathbf{n}(\mathbf{s}')$ denotes the normal vector of the surface at the position $\mathbf{s}'$. It is essential to take into account the second term on the r.h.s. of (2). Only in very special cases, for example, if a simple poloidal flow is exposed to an axial magnetic field so that the induced current flows only in azimuthal direction, this second term is zero. If, however, a purely azimuthal flow is exposed to an axial field, the second term completely cancels out the first term. Utilizing the fact that **j** is divergence-free, one can derive from (1) a Poisson equation for the electric potential whose solution also fulfills the boundary integral equation

$$\varphi(\mathbf{s}) = \frac{1}{2\pi}\int_D \frac{\big(\mathbf{u}(\mathbf{r}')\times\mathbf{B}(\mathbf{r}')\big)\cdot(\mathbf{s}-\mathbf{r}')}{|\mathbf{s}-\mathbf{r}'|^3}\,dV' - \frac{1}{2\pi}\oiint_S \varphi(\mathbf{s}')\;\frac{\mathbf{s}-\mathbf{s}'}{|\mathbf{s}-\mathbf{s}'|^3}\cdot\mathbf{n}(\mathbf{s}')dS' \tag{3}$$

if insulating boundaries are assumed.

In general, the total magnetic field **B** under the integrals of (2) and (3) is the sum of an externally applied primary magnetic field $\mathbf{B}_0$ and the induced secondary magnetic field **b** itself. In magnetohydrodynamics, the ratio between **b** and $\mathbf{B}_0$ is known to be proportional to the magnetic Reynolds number *Rm*, defined as

$$Rm = \mu_0\sigma LU \tag{4}$$

with *L* and *U* denoting characteristic length and velocity scales of the fluid, respectively. For large values of *Rm* and suitable flow topologies, it is possible to achieve self-excitation of a magnetic field. Such homogeneous dynamos have indeed been studied [6,7] by solving the integral equation system (2) and (3). However, in most industrial applications *Rm* is smaller than 1. To take continuous casting of steel as a typical example, with a mould width of 1 m, a typical flow velocity of 0.1 m/s, and a conductivity of the liquid steel of $7 \cdot 10^5$ S/m, we arrive approximately at *Rm*= 0.1. In such cases, **B** can be replaced by $\mathbf{B}_0$ under the integrals in (2) and (3). In this approximation, we get a linear inverse problem for the determination of the velocity field **u** from the induced magnetic field **b** measured in the exterior of the fluid. Of course, the unknown electric potential at the fluid boundary must not be neglected and has to be treated in due manner.

Assume now *K* different external magnetic fields $\mathbf{B}_0^k$ to be applied to the fluid. Suppose, for each $\mathbf{B}_0^k$, all measured induced magnetic field components to be collected into an N_b-dimensional vector

with the entries b_i^k . Accordingly, the discretized electric potential at the surface S is collected into an N_φ-dimensional vector with the entries φ_m^k, and the desired velocity **u** in the volume V is discretized as an N_V-dimensional vector with the entries u_l. Then, (2) and (3) can formally be written in the form:

$$b_i^k = K_{il}^k u_l + L_{im}\varphi_m^k \tag{5}$$

$$\varphi_m^k = M_{ml}^k u_l + N_{mn}\varphi_n^k \tag{6}$$

Note that only the matrices $\mathbf{K}^k$ and $\mathbf{M}^k$ depend on the applied magnetic field $\mathbf{B}_{0,k}$, whereas the matrices **L** and **N** depend on the geometry only. A peculiarity of equation (6) is well known from magnetoencephalography (MEG) [8]. Actually, the matrix (**I** − **N**) is singular which indicates the fact that the electric potential is defined only up to an additional constant. This problem can be circumvented by using the so-called deflation method [8], replacing (**I** − **N**) by the well-conditioned matrix $(\mathbf{I} - \mathbf{N})^{\mathrm{defl}}$. Inserting the solution of (deflated) equation (6) into (5) we end up with a single linear relationship between the desired velocity field and the measured magnetic field in the form

$$b_i^k = K_{il}^k u_l + L_{im}(I-N)_{mn}^{-1,defl} M_{nl}^k u_l \tag{7}$$

For further details of the numerical solution of this equation, in particular concerning the accurate computation of the boundary integrals, see [9].

We can now derive the velocity by solving the normal equations arising from the minimization of the following total functional of the velocity field:

$$F[\mathbf{u}] = \sum_{k=1}^{K} F_k[\mathbf{u}] + F_{\mathrm{div}}[\mathbf{u}] + F_{\mathrm{pen}}[\mathbf{u}] \tag{8}$$

with

$$F_k[\mathbf{u}] = \sum_{i=1}^{N_b} \frac{1}{\sigma_{i,k}^2}\left(b_{i,\mathrm{meas}}^k - b_{i,\mathrm{model}}^k[\mathbf{u}]\right)^2 \tag{9}$$

$$F_{\mathrm{div}}[\mathbf{u}] = \frac{1}{\sigma_{\mathrm{div}}^2}\sum_{l=1}^{N_V} (\nabla\cdot\mathbf{u})_l^2 \Delta V_l \tag{10}$$

$$F_{\mathrm{pen}}[\mathbf{u}] = \frac{1}{\sigma_{\mathrm{pen}}^2}\sum_{l=1}^{N_V} \mathbf{u}_l^2 \Delta V_l \tag{11}$$

where ΔV_l denotes the volume of the element at the volume grid point l. The first sum over the functionals $F_k[\mathbf{u}]$ is the most essential one as it represents the mean squared residual deviation of the measured magnetic fields $b_{i,\mathrm{meas}}^k$ from the fields $b_{i,\mathrm{model}}^k$ modeled according to (7).

The functional $F_{\mathrm{div}}[\mathbf{u}]$ enforces the velocity field to be solenoidal, and the last functional $F_{\mathrm{pen}}[\mathbf{u}]$ is the regularization (penalty) functional which tries to minimize the kinetic energy. The parameters $\sigma_{i,k}$ are the a priori errors for the measured induced magnetic fields. σ_{div} is chosen very small in order to ensure the divergence-free condition. The parameter to play with in the regularization procedure is σ_{pen}. Here we employ the so-called Tikhonov regularization [3]: by increasing the regularization parameter σ_{pen}, one obtains solutions of the inverse problem with increasing kinetic energy of the flow. The optimal solution is then found at the point of strongest curvature of Tikhonov's L-curve which is done by an automatic search described in [9].

The above equation system (7-11) is valid for the case of different applied magnetic fields and a fully three-dimensional (3D) flow. It can, however, also be adapted to the essentially two-dimensional (2D) case of slab-casting, where only one magnetic field B_0 is applied. In this case, the dimensional

reduction of the velocity structure from 3D to 2D can be realized by adding an additional functional which enforces the velocity to be 2D. Optionally, any available prior information, e.g. on the velocity at the inlet which is available from the casting speed, can also be considered by including a further appropriate quadratic functional into (8).

It should be noted that regularization based on some reasonable norm of the velocity is actually more than only a trick since in most cases the assumption of a rather smooth velocity field is sensible from a physical point of view. For the same reason it is clear, however, that the method is not suited to detect very small vortices in a strongly turbulent flow (see [4,5] for the corresponding uniqueness problem).

3. A three-dimensional flow reconstruction problem

The aim of a first demonstration experiment [1] for CIFT was to reconstruct a propeller-driven three-dimensional flow of a liquid metal in a compact cylindrical vessel (see Figure 1(a)). The flow of the eutectic alloy GaInSn was stirred by a motor driven propeller with a diameter of 6 cm inside a cylindrical polypropylene vessel with radius R = 9 cm and height 17.2 cm.

For determining both the poloidal flow (in radial and axial direction) and the toroidal flow (in azimuthal direction), we applied subsequently a vertical $B_{0,z}$ and a horizontal $B_{0,x}$ magnetic field, both produced by Helmholtz-like coil pairs. The switching between the two fields occured every 3 seconds, so that after 6 seconds all the magnetic field information was available for the velocity reconstruction. This time resolution could be significantly enhanced, with a physical limitation given by the magnetic decay time $\mu_0\sigma R^2$, which is in the order of 0.05 s for the demonstration experiment.

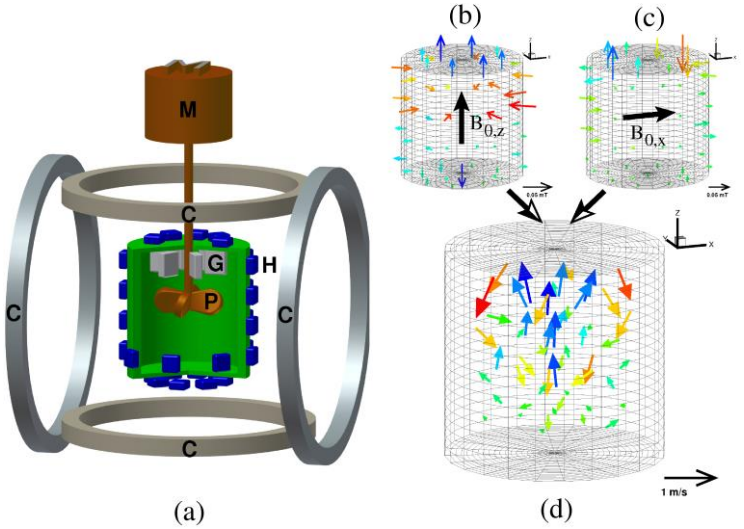

Figure 1. (a) Schematic sketch of the experiment for the validation of CIFT at a propeller driven 3D flow using GaInSn. M—motor, C—coils, P—propeller, G—guiding blades, and H—Hall sensors. (b) Measured induced field at 48 positions for upward pumping propeller for applied $B_{0,z}$. The arrows indicate the field component measured by the Hall sensors. (c) Same as (b), but for applied $B_{0,x}$. (d) Velocity field as reconstructed by CIFT from (b) and (c).

For each of the two applied fields $B_{0,z}$ and $B_{0,x}$ the components of the induced fields normal to the surface were measured at 48 positions, which are rather homogeneously distributed all over the surface of the cylindrical vessel. For the measurement KSY 44 Hall sensors (Infineon) were used. The small ratio of around $10^{-3}\ldots10^{-2}$ between the induced and the applied fields requires a stable current source of the Helmholtz-like coils, a very stiff relative position of Hall sensors and coils, and

significant effort to compensate drift and sensitivity changes of the Hall sensors (e.g., due to varying temperature).

By inverting the measured induced magnetic fields, it was possible to clearly distinguish between upward and downward pumping of the propeller, with the rotational component being deliberately reduced by guiding blades in the case of upward pumping. For this particular case, Figures 1(b) and 1(c) show the measured induced fields for applied $B_{0,z}$ and $B_{0,x}$, respectively, and Figure 1(d) depicts the velocity field as reconstructed from these two sets of information. The comparison with UDV measurements had shown a good coincidence of the resulting velocity fields [1]. Later, an independent confirmation of the flow structure was obtained by Lorentz force velocimetry [10].

4. Application to slab casting problems

We now move from the general 3D flow reconstruction problem to a problem which can be treated as a 2D problem. In the continuous casting of steel slabs, the liquid metal flows from a tundish through a submerged entry nozzle (SEN), with typically two sideward directed ports at the lower end, into the mould where it starts to solidify at the water cooled copper walls. The flow structure in the mould is known to play a key role for the quality of the produced steel [11]. A stable double-roll flow structure, in which the two jets emanating from the SEN ports first reach the narrow-faces of the mould and then split into upward and downward directed branches, is considered as most desirable. The so-called single-roll structure, however, with the jets being sharply bent upward after leaving the SEN ports, represents a danger since it could lead to entrainment of casting powder into the steel. Any sort of online-monitoring of the detailed flow-structure in the mould would be helpful for an active control of the casting process, with the prospect to increase the possible casting speed significantly. As a contactless method, CIFT suggests itself for such monitoring, although various problems connected with copper-mould oscillations and the use of coatings with ferromagnetic Nickel makes its implementation in the industry still a formidable task.

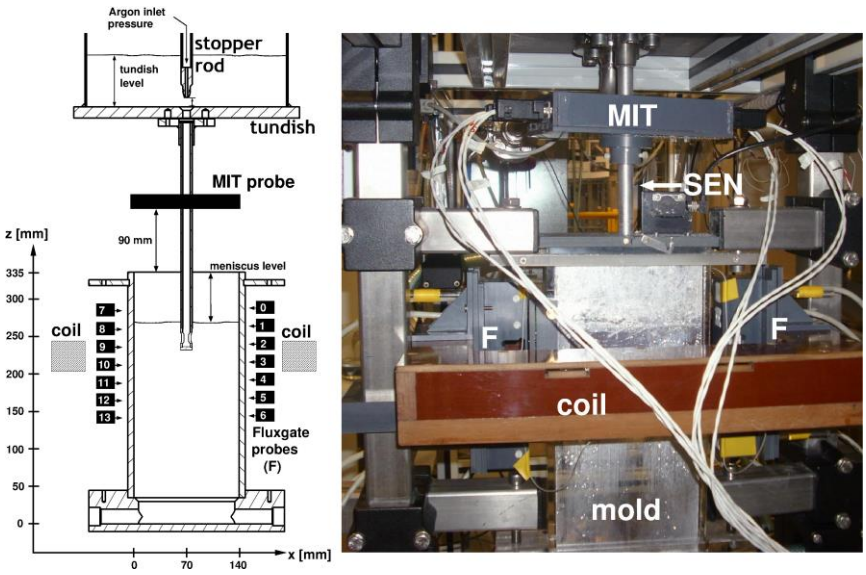

Figure 2. Schematic sketch (left) and photography (right) of the central part of the Mini-LIMMCAST facility.

As a very first step in this direction, we have installed a simplified CIFT system at the small continuous casting model Mini-LIMMCAST, working also with the GaInSn alloy (Figure 2). The simplification concerns the restriction of the CIFT system to a single magnetic field coil which

produces a mainly vertical magnetic field. This configuration is sufficient for the determination of the velocity component parallel to the wide faces of the mould [12], which is indeed the dominant one for the particular case of slab-casting. The induced fields are measured by fluxgate sensors positioned at the narrow faces of the mould, typically at 7 positions on either side. In addition to CIFT, we have utilized a mutual inductance tomography (MIT) system for determining the conductivity distribution in the SEN, which allows visualizing the details of the two-phase GaInSn/Argon flow [13,14]. The simultaneous utilization of CIFT and MIT leads to a detailed understanding of the two-phase flow in the SEN and of the resulting flow in the mould [15]. Figure 3 illustrates two typical flow structures that had been detected during one run of the experiment, i.e. double-roll and single-roll structures occurring on different sides of the mould.

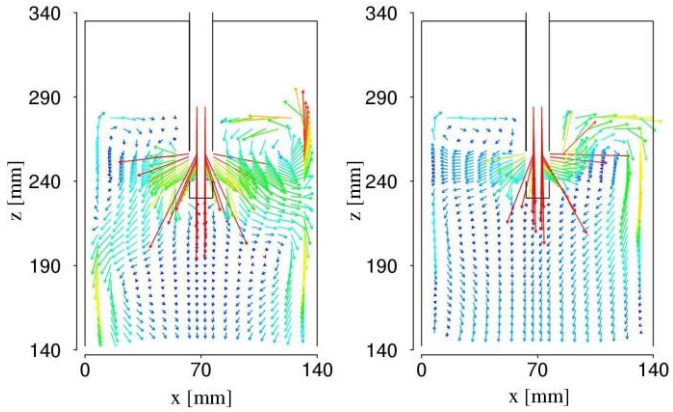

Figure 3. CIFT-reconstructed velocity obtained at the Mini-LIMMCAST facility, for the case that Argon is being injected at the top of the SEN. At one instant, the desired double role structure (left) appears, somewhat later, and the undesired single role structure dominates (right).

5. CIFT in presence of a strong electromagnetic brake

For decades, electromagnetic brakes (EMBrs) have been used with the goal to stabilize the flow in the mould and to dampen its oscillations, while recent experiments have challenged this simple view [16]. One might ask whether CIFT is able to work even under the extreme condition that a strong static magnetic field is applied in addition to the measuring field. Some related experiments were conducted at the Mini-LIMMCAST slab caster model. A ruler-type brake was used to generate a DC magnetic field perpendicular to the wide faces of the mould and hence to the main flow direction (Figure 4). Under these circumstances it was necessary to enhance the emitting system by a second coil. The induced magnetic fields were measured with 2 × 7 cylindrical induction coils positioned at the narrow faces of the caster model (the presence of the strong brake field prohibits the use of fluxgate sensors which would saturate approximately at 2 mT). Each induction coil has 340,000 windings with a conductor diameter of 25 μm. The signals from the coils were digitized by a 24-bit ADC from LTT Tasler. In the post-processing step the amplitude and the phase of the signal in comparison to the current through the excitation coil is calculated using the quadrature demodulation.

Figure 5 shows the time-dependence of the measured magnetic fields at the 2 × 7 positions for three different settings. Figure 5a corresponds to the case that the brake field is switched off. Figure 5b corresponds to the case that a brake field of 300 mT is switched on, and the walls of the "mould" are insulating. Apart from an overall change of the structure of the induced field (which reflects an upward shift of the jet), we also observe a slow oscillation (with a typical period of 5 seconds). This confirms the observations of [16] that the magnetic brake, contrary to previous expectations, can indeed lead to stronger fluctuations. Finally, figure 5c shows the signal for switched-on brake field,

this time however, with conducting walls. Evidently the long period oscillations have disappeared, again in agreement with [16].

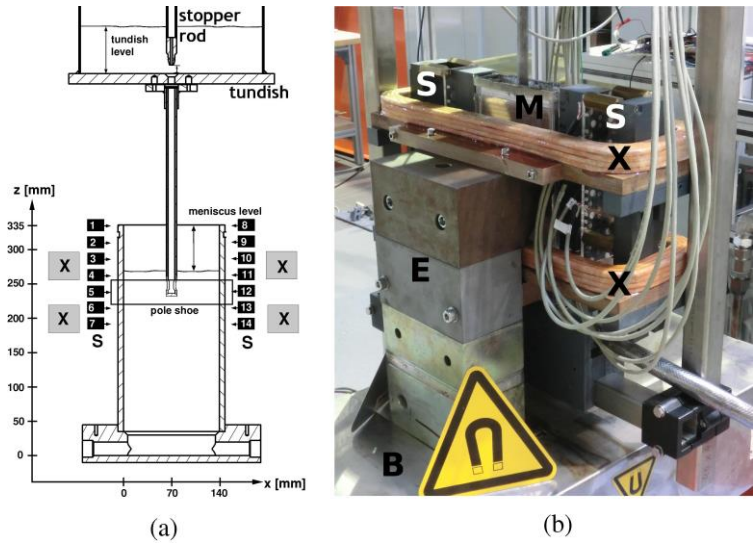

Figure 4. Schematic sketch (left) and photography (right) of the central part of the Mini-LIMMCAST facility with a ruler-type electromagnetic brake applied, and an enhanced emitter coil system. X—two emitter coils, S—sensor system, E— EMBr, B—brake coils.

While more detailed investigations of these effects are still necessary, it is quite remarkable that on the background of a strong brake field of 300 mT it is possible to measure safely the induced magnetic fields which are 6-7 orders of magnitude smaller and to reconstruct from them the velocity.

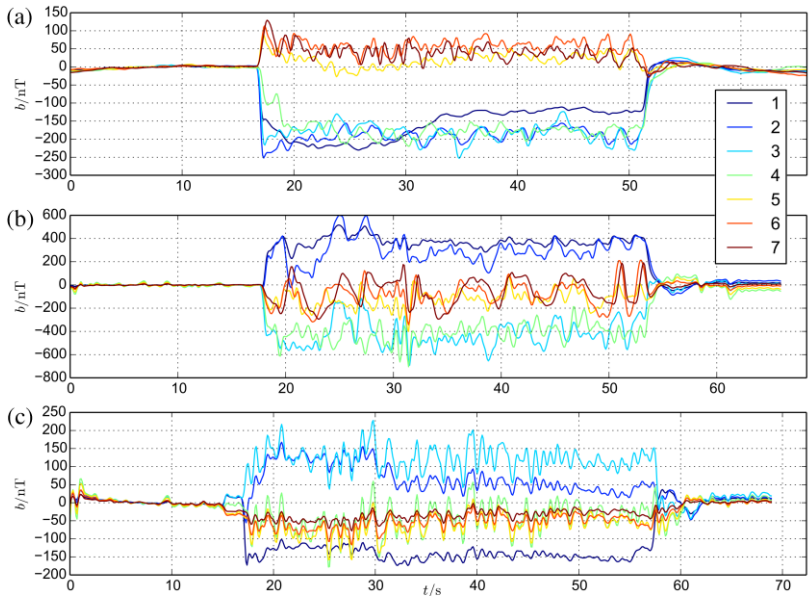

Figure 4. Measurements of the induced magnetic field for the magnetic brake switched off (a), switched on with insulating walls (b), and with conducting walls (c).

6. Outlook

Future work will be devoted to adapting CIFT for its deployment under the harsh mechanical and electromagnetic conditions in a real casting plant. A main challenge is certainly the up-and-down oscillation of the copper mould. Even if the measuring coil, together with the sensors, could be stably installed at the mould, one has to be aware of disturbing induction effects due to the relative motion of the mould to the rest of the facility. A further problem is posed by the widely used Nickel coating of the copper could. At present it is not clear whether or not the magnetic field deformations due to the magnetic properties of Nickel can be mastered.

Another possible application of CIFT, beyond steel casting, may be the Czochralski crystal growth of silicon. First tests have already been made at various pullers. On the laboratory scale, CIFT-like flow inference methods have also been applied for the identification of current-driven instabilities [17] with relevance for liquid metal batteries, and for the flow reconstruction in a Rayleigh-Bénard cell with liquid metal.

Another project for the future is to combine into one single scheme the CIFT method with the mutual inductance tomography. A simultaneous but yet spatially separated application of both methods at the Mini-LIMMCAST facility was already documented in [13,14]. The question is whether both conductivity variation and the velocity field could be obtained by one single measurement system. A first step in this direction was the reformulation of CIFT in terms of the sensitivity matrix [18].

7. Acknowledgments

This work was supported by Helmholtz-Gemeinschaft Deutscher Forschungszentren (HGF) in frame of the Helmholtz Alliance LIMTECH.

8. References

[1] Stefani F, Gundrum T and Gerbeth G 2004 *Phys. Rev. E* **70** 056306
[2] Hansen PC 1992 *SIAM Rev.* **34** 561
[3] Stefani F and Gerbeth G 1999 *Inverse Probl.* **15** 771
[4] Stefani F and Gerbeth 2000 *Inverse Probl.* **16** 1
[5] Stefani F and Gerbeth G 2000 *Meas. Sci. Techn.* **11** 758
[6] Stefani F, Gerbeth G and Rädler KH 2000 *Astron. Nachr.* **321** 65
[7] Xu M, Stefani F and Gerbeth G 2004 *J. Comp. Phys.* **196** 102
[8] Hämäläinen R et al. 1993 *Rev. Mod. Phys.* **65** 413
[9] Wondrak T, Stefani F, Gundrum T and Gerbeth G 2009 *Int. J. Appl. Electromagn. Mech.* **30** 255
[10] Heinicke C and Wondrak T 2014 *Meas. Sci. Techn.* **25** 055302
[11] Zhang L, Yang S, Cai K, Li J and Thomas BG 2007 *Met. Mater. Trans. B* **38** 63
[12] Wondrak T et al. 2010 *Meas. Sci. Tech.* **21** 045402
[13] Terzija N et al. 2011 *Flow Meas. Instr.* **22** 10
[14] Terzija N et al. 2011 *Meas. Sci. Techn.* **22** 015501
[15] Wondrak T et al. 2011 *Met. Mater. Trans. B* **42** 1201
[16] Timmel K, Eckert S and Gerbeth G 2011 *Met. Mater. Trans. B* **42** 68
[17] Seilmayer M et al. 2012 *Phys. Rev. Lett.* **108** 244501
[18] Yin W, Peyton AJ, Stefani F and Gerbeth G 2009 *Meas. Sci. Tech.* **20** 105503